JOURNAL OF THE ROYAL SOCIETY Interface

CrossMark click for updates

J. R. Soc. Interface (2012) **9**, 2997–3007
doi:10.1098/rsif.2012.0314
Published online 6 June 2012

Immunofluorescence-guided atomic force microscopy to measure the micromechanical properties of the pericellular matrix of porcine articular cartilage

Rebecca E. Wilusz[1,2], Louis E. DeFrate[1,2] and Farshid Guilak[1,2,*]

[1]*Department of Orthopaedic Surgery, Duke University Medical Center, Box 3093, Durham, NC 27710, USA*
[2]*Department of Biomedical Engineering, Duke University, Durham, NC 27708-0281, USA*

The pericellular matrix (PCM) is a narrow region that is rich in type VI collagen that surrounds each chondrocyte within the extracellular matrix (ECM) of articular cartilage. Previous studies have demonstrated that the chondrocyte micromechanical environment depends on the relative properties of the chondrocyte, its PCM and the ECM. The objective of this study was to measure the influence of type VI collagen on site-specific micromechanical properties of cartilage *in situ* by combining atomic force microscopy stiffness mapping with immunofluorescence imaging of PCM and ECM regions in cryo-sectioned tissue samples. This method was used to test the hypotheses that PCM biomechanical properties correlate with the presence of type VI collagen and are uniform with depth from the articular surface. Control experiments verified that immunolabelling did not affect the properties of the ECM or PCM. PCM biomechanical properties correlated with the presence of type VI collagen, and matrix regions lacking type VI collagen immediately adjacent to the PCM exhibited higher elastic moduli than regions positive for type VI collagen. PCM elastic moduli were similar in all three zones. Our findings provide further support for type VI collagen in defining the chondrocyte PCM and contributing to its biological and biomechanical properties.

Keywords: chondron; proteoglycan; scanning probe microscope; indentation

1. INTRODUCTION

Articular cartilage is the connective tissue that lines the articulating surfaces of diarthrodial joints, providing a low-friction, load-bearing surface that supports and distributes the forces generated during joint motion. The functional mechanical properties of cartilage are conferred by the tissue's extensive extracellular matrix (ECM) that is produced and maintained by a single population of cells known as chondrocytes. During joint activity, chondrocytes are subjected to a complex mechanical environment consisting of temporal and spatial variations in stress and strain, hydrostatic pressure, streaming potentials and osmotic pressure [1–3]. This mechanical environment has been shown to significantly impact the balance of chondrocyte anabolic and catabolic activities, and in turn, influence the overall health of the joint (reviewed in earlier studies [4–6]).

*Author for correspondence (guilak@duke.edu).

Electronic supplementary material is available at http://dx.doi.org/10.1098/rsif.2012.0314 or via http://rsif.royalsocietypublishing.org.

Within the ECM, chondrocytes are surrounded by a narrow region called the pericellular matrix (PCM), which together with the enclosed cell(s), is termed the chondron [7]. In normal cartilage, the PCM is often defined by the exclusive presence and localization of type VI collagen around the chondrocytes [8–11] and is characterized by an elevated concentration of proteoglycans and glycoproteins relative to the surrounding ECM [12–14]. While the exact function of the PCM in cartilage is not fully understood, it is thought to play an important biomechanical role in the tissue. It has been hypothesized that each chondrocyte tailors its PCM on the basis of a unique set of dynamic mechanical forces at its position within the matrix [8], suggesting that the PCM serves to protect the chondrocyte during compressive loading [7] and to act as a transducer of mechanical and biochemical signals in the cellular microenvironment [15]. Furthermore, the relationship between the molecular constituents of the PCM (e.g. type VI collagen) and its mechanical properties are not fully understood.

Previous theoretical models [16–19] and experimental studies [20–24] have demonstrated a functional

Received 16 April 2012
Accepted 14 May 2012

biomechanical role for the PCM. In particular, the stress–strain environment of the chondrocyte heavily depends on the relative mechanical properties of the chondrocyte, its PCM, and the local ECM [16,17,23]. Cartilage is subdivided into three zones (superficial, middle and deep) based on the depth from the articular surface that are characterized by differences in ECM composition and ultrastructure [14,25–27] and chondrocyte morphology and arrangement [12,28]. Zonal variations in matrix composition and structure contribute to a depth-dependent increase in compressive properties of the cartilage ECM [29–31]. Isolated chondrocytes also demonstrate zonal differences in their mechanical properties, with superficial zone cells exhibiting higher moduli than do middle/deep zone cells [32,33]. While the three-dimensional morphology and thickness of the PCM varies among the cartilage zones [11,14], micropipette aspiration of mechanically isolated chondrons from canine [34] and human [35,36] cartilage revealed zonal uniformity in the mechanical properties of the PCM, despite significant zonal differences in ECM properties. Although recent studies have evaluated the biomechanical properties of the cartilage PCM *in situ* indirectly using an inverse boundary element analysis coupled with three-dimensional confocal microscopy [37] and directly by atomic force microscopy (AFM) [38], the existence (or lack) of zonal variation in PCM properties *in situ* has yet to be determined.

AFM has emerged as a powerful tool for biomechanics applications because it provides a means for precisely controlling nano- and microindentation in aqueous environments. Using a force spectroscopy technique known as stiffness or force-volume mapping, AFM can be used to collect arrays of indentation curves and map spatial variations in elastic modulus over a specified region [39–41]. In this regard, AFM indentation has been used to investigate the mechanical properties of local features in multiple cartilaginous tissues, including intervertebral disc [42], fibrocartilage [43], growth plate [44,45] and articular cartilage [31,38,46–49]. More recently, AFM has been combined with a number of optical microscopy techniques, including phase contrast and fluorescence [50,51], allowing for simultaneous stiffness mapping and high-resolution imaging, thereby providing a means for direct correlation between structural features, biochemical composition and biomechanical properties.

The objective of this study was to characterize the mechanical properties of the ECM and PCM in the microenvironment of the chondrocyte *in situ* by using AFM and test the hypotheses that the biomechanical properties of the PCM correlate with the presence of type VI collagen and are uniform with depth from the articular surface. PCM regions in cryosections of full-thickness articular cartilage samples from porcine knees were identified using fluorescence immunolabelling for type VI collagen. Guided by this biochemical definition of the PCM, we used AFM stiffness mapping [38] to evaluate the elastic properties of matched PCM and ECM regions within the superficial, middle and deep zones *in situ* and to correlate these properties to the presence of type VI collagen.

2. METHODS

2.1. Tissue sample preparation

Full-thickness articular cartilage samples were collected from central regions of the medial femoral condyle of 2- to 3-year-old, skeletally mature, female pig knee joints with no macroscopic signs of joint degeneration. Cartilage samples were wrapped in phosphate-buffered saline-soaked gauze and frozen at -20°C for intermediate storage. Samples were embedded in water-soluble embedding medium (Tissue-Tek O.C.T. Compound; Sakura Finetek USA, Inc., Torrance, CA, USA) and sectioned perpendicular to the articular surface in 5-μm-thick slices using a cryostat microtome (Leica CM1850; Leica Microsystems, Inc., Buffalo Grove, IL, USA). Cartilage slices were collected on negatively charged glass slides and washed thoroughly with 0.1 M tris-buffered saline (TBS; pH 7.3) to remove the water-soluble embedding medium prior to immunofluorescence (IF) labelling and AFM testing.

2.2. Immunofluorescence for type VI collagen

Unfixed cartilage sections were labelled for type VI collagen, using a modified IF protocol [11]. At room temperature, sections were blocked for 20 min in 10 per cent normal donkey serum (lot no. S10011325; Fitzgerald Industries International Inc., Acton, MA, USA) diluted in assay buffer (0.1% bovine albumin solution, BSA; Invitrogen, Carlsbad, CA, USA) in 0.1 M TBS, pH 7.3). Samples were incubated with primary antibody for type VI collagen (anti-collagen type VI raised in rabbit, 70R-CR009X, Fitzgerald) at a 1 : 50 dilution in 10 per cent donkey serum for 20 min at room temperature. After two TBS washes of 5 min each, samples were incubated in a dark room, using secondary antibody (FITC-conjugated donkey anti-rabbit IgG, 43R-ID061FT; Fitzgerald) at a 1 : 200 dilution in 10 per cent donkey serum for 20 min at room temperature. During AFM testing, sections were rinsed twice in TBS for 5 min each and allowed to remain in TBS at room temperature.

2.3. Mechanical characterization via atomic force microscopy

Simultaneous force measurements and fluorescence imaging were carried out using an AFM system (MFP-3DBio; Asylum Research, Santa Barbara, CA, USA) integrated with an inverted fluorescence microscope (AxioObserver A1; Carl Zeiss, Inc., Thornwood, NY, USA). For microscale indentation, borosilicate glass spheres (diameter 5 μm) were attached to tip-less AFM cantilevers ($k \approx 4.5\ \mathrm{N\ m^{-1}}$; Novascan Technologies, Inc., Ames, IA, USA). Indentations were applied with a force trigger of 300 nN, and curves were sampled at 7.5 kHz. For evaluation of PCM elastic properties, indentations (1600 sites per region, 15 $\mu\mathrm{m\ s^{-1}}$ indentation velocity) were sequentially applied over a 20×20 μm region of interest defined by a microscopic examination with phase contrast imaging (figure 1*a*) and positive IF labelling for type VI collagen around cell-sized voids (figure 1*b*). Topographical maps of relative height were

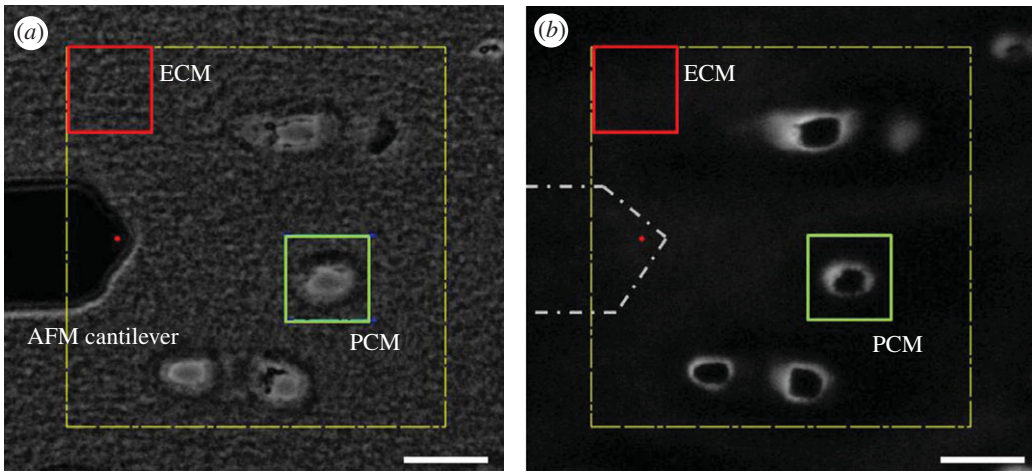

Figure 1. (*a*) Phase contrast and (*b*) fluorescence images illustrating the selection of PCM and ECM testing regions in the deep zone of porcine cartilage as seen during AFM testing. Localization of type VI collagen immediately surrounding cell-sized voids was used to identify the PCM in IF-labelled samples. The AFM cantilever is shown in (*a*) and outlined in (*b*), with the red circle indicating the approximate location of the spherical tip. Scale bars, (*a*,*b*) 20 μm. (Online version in colour.)

collected simultaneously during stiffness mapping of each PCM scan region. Elastic properties of the adjacent ECM were evaluated using the same approach over 20 × 20 μm regions visually devoid of PCM and type VI collagen ([16] indentations per region, 15 μm s^{-1} indentation velocity).

In order to investigate the potential influence of IF labelling on measured microscale elastic properties, site-matched PCM/ECM regions (total regions, $n = 17$) were evaluated in the middle/deep zone (200–400 μm from articular surface) of paired unlabelled and IF-labelled cartilage sections ($n = 3$ pigs). Unlabelled sections underwent minimal washing to remove the water-soluble embedding medium and underwent AFM testing immediately. AFM testing was conducted in TBS at room temperature and was completed within 4 h of initial sectioning. Preliminary studies showed no significant changes in the mechanical properties or Safranin-O staining of proteoglycans in IF-labelled cartilage sections over the time course of AFM testing (113 ± 18 kPa versus 94 ± 11 kPa, $p = 0.39$, Student's *t*-test).

To evaluate zonal variations in PCM elastic properties *in situ*, paired PCM/ECM regions ($n = 5$ pigs, $n = 20$ total regions per zone) were selected within each of the three cartilage zones. The superficial zone was defined to include the region 0–100 μm from the articular surface, the middle zone as 200–300 μm from the articular surface and the deep zone as the bottom half of each cartilage section. These designations were selected based on variations in cell morphology and tissue architecture outlined in the literature [26,27]. The order of testing among the three zones was varied among the cartilage samples. All AFM testing was conducted in TBS at room temperature and completed within 4 h of initial sectioning.

2.4. Data evaluation

Raw data for cantilever deflection and z-piezo movement were collected and analysed using a custom MATLAB script (The MathWorks, Natick, MA, USA). The elastic modulus, E, was determined by fitting a modified Hertz model to force–indentation curves, as described previously [32]. For articular cartilage, the local Poisson's ratio, ν, was assumed to be 0.04 for both the ECM [23,30,52] and PCM [36] based on previous experimental reports in the literature. From the Hertz model, the presented modulus values can be converted from $\nu = 0.04$ to a different assumed value of ν by multiplying by the conversion factor $(1 - \nu^2)/(1 - 0.04^2)$. Probe–surface contact was identified using contact point extrapolation, a method that uses the indentation portion of the approach curve to determine the probe–surface contact point on soft substrates on the basis of an applied mathematical model [53]. Hertzian contact mechanics provided excellent fits to the experimental data for all force–indentation curves ($r^2 > 0.90$). Two-dimensional contour maps were generated of the spatial distribution of calculated elastic moduli in each region.

To compare the elastic moduli of unlabelled and IF-labelled PCM, a distance-based definition of the PCM was used as described previously [38]. Briefly, PCM regions were determined based on spatial indicators of contact with the underlying glass substrate within cell-sized voids. Glass contact was readily apparent from the force–indentation curves and was used to define the edge of each cell void. PCM data were included for a region extending 1 μm radially from this edge. This defined region may locally under- or over-represent the actual extent of the PCM for any given site but provided a consistent definition of the PCM among samples in the absence of IF labelling.

For IF-labelled sections, the cartilage PCM was identified by positive type VI collagen staining around cell-sized voids, and data were included for all indentations that fell within labelled regions. For precise navigation, using the AFM MFP-3D software (Asylum Research), the tip location on the AFM cantilever must be specified. Because the spherical tip was not visible in either captured light or fluorescence images, its location was approximated to be within 2–3 μm (figure 1), and an image analysis algorithm was

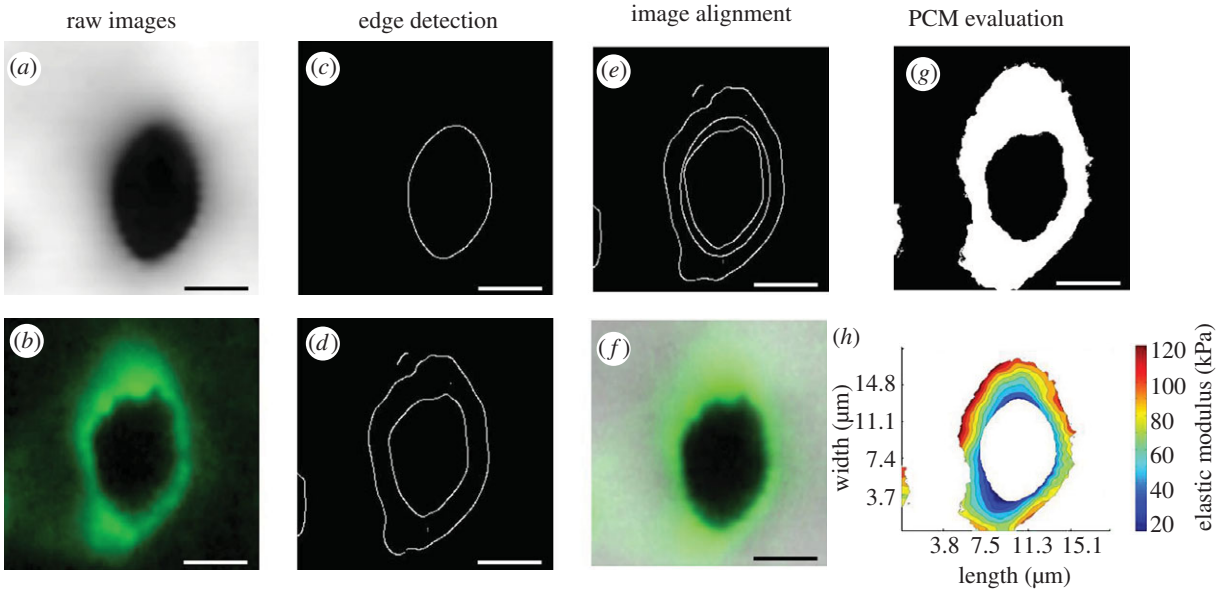

Figure 2. An image analysis was performed in MATHEMATICA to align stiffness maps and IF images for PCM data analysis. The inner edge of cell-sized voids was detected in (*a*) topographical maps and (*b*) IF images using (*c*,*d*) edge detection. The topographical map was translated in the *x*- and *y*-directions to minimize the distance between it and the IF image (*e*). Stiffness maps and IF images were cropped for alignment as needed (shown overlaid in *f*). Aligned IF images were thresholded and converted to binary masks to determine regions of positive IF-labelling (*g*). IF-positive masks and elastic moduli contour maps were analysed in MATLAB to extract PCM moduli from each scan region (*h*). Scale bars, 5 μm. (Online version in colour.)

developed in MATHEMATICA (Wolfram Research, Inc., Champaign, IL, USA) to correct for any translational shift between captured IF images and stiffness maps. IMAGEJ (National Institutes of Health) was used to crop AFM navigation images (figure 1*b*) and produce an IF image of each PCM scan region (figure 2*b*; 256 × 256 pixels) that was imported into MATHEMATICA. The corresponding topographical (figure 2*a*) and elastic moduli contours maps (not shown) were resized from 40 × 40 pixels to 256 × 256 pixels using bilinear interpolation. The topographical map was used for alignment of stiffness maps owing to its clear depiction of the cell-sized void associated with each PCM. Because indentation points on the topographical map perfectly align with points on the elastic moduli contour map, any translational shift in the topographical map could be directly applied to the contour map. Edge detection was used to define the inner edge of the cell-sized void in the topographical map and IF image (figure 2*a*–*d*). Using an iterative closest-point technique [54], the topographical map was translated in the *x*- and *y*-directions to minimize the distance between the cell void inner edge in the topographical map and IF image. With the magnitude of the translational shift between the two images determined, the IF image and elastic moduli contour maps were cropped as necessary to align the images (figure 2*e*,*f*). Once aligned, IF images were converted to binary masks to indicate regions of positive IF labelling using an optimal threshold value determined from a range of images (figure 2*g*). IF-positive masks and elastic moduli contour maps were analysed in MATLAB to extract PCM data from each scan region (figure 2*h*). To quantitatively evaluate the spatial distribution of moduli in the chondrocyte microenvironment, the stiffness progression from the PCM outer edge to the ECM was evaluated in radial increments of 0.5 μm.

2.5. Statistical analyses

Differences in ECM and PCM elastic moduli between unlabelled and IF-labelled cartilage sections were evaluated using a two-way ANOVA (region, label; $\alpha = 0.05$), and Fisher's least significant difference (LSD) post hoc test. Differences between ECM and PCM elastic moduli among the three zones were evaluated using a two-way ANOVA (region, zone; $\alpha = 0.05$) and Fisher's LSD post hoc test. Differences in PCM elastic moduli among the three zones were evaluated separately using a one-way ANOVA ($\alpha = 0.05$). Stiffness progression data were evaluated separately within each zone using a one-way ANOVA (distance, $\alpha = 0.05$) and Fisher's LSD post hoc test. The relationship between elastic modulus and fluorescence intensity for each PCM scan region was determined using linear regression.

3. RESULTS

Immunolabelling of cartilage sections for type VI collagen showed clear localization of type VI collagen to the regions immediately surrounding cell-sized voids. In the superficial zone, cell-sized voids and their associated PCM were elongated parallel to the articular surface (figure 3*a*). In the middle zone, the PCM and cell voids exhibited a more rounded morphology (figure 3*b*). In the deep zone, cell-sized voids and their associated PCM were elongated perpendicular to the articular surface (figure 3*c*).

The influence of IF labelling on the observed microscale mechanical properties was evaluated in the

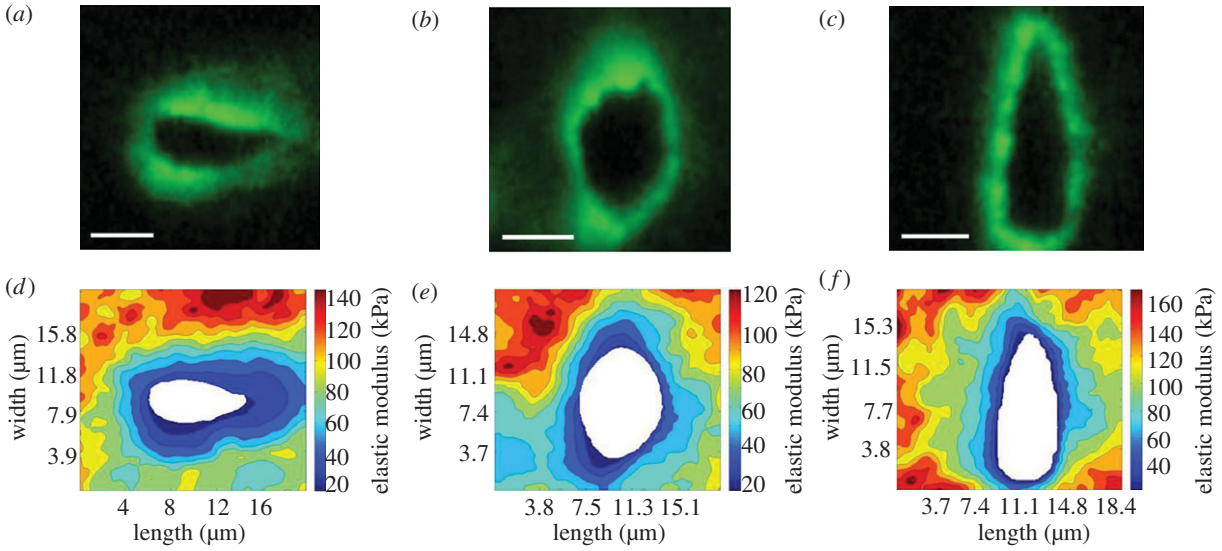

Figure 3. Stiffness mapping of the PCM in the (*a*,*d*) superficial, (*b*,*e*) middle and (*c*,*f*) deep zones of articular cartilage. (*a*–*c*) Representative IF images showing the distribution of type VI collagen around cell-sized voids in each zone. (*d*–*f*) Representative contour maps of calculated elastic moduli of PCM scan regions in each zone. The spatial distribution of type VI collagen co-localized with softer modulus regions within each scan. Scale bars, 5 μm. (Online version in colour.)

middle/deep zone of unlabelled and IF-labelled cartilage sections. No significant difference was observed in the measured elastic moduli in either the predefined 1 μm PCM region or the ECM with IF labelling ($p = 0.97$ for PCM, $p = 0.39$ for ECM; figure 4). ECM elastic moduli were significantly greater than PCM elastic moduli in both unlabelled and labelled sections ($p < 0.001$).

Stiffness mapping revealed that type VI collagen and lower elastic moduli co-localized in the pericellular space around cell-sized voids (figure 3). Regions exhibiting higher fluorescence intensity had lower elastic moduli (figure 5). There was a significant relationship between fluorescence intensity and elastic modulus within PCM scan regions ($p < 0.0001$). The strongest relationships, based on r^2, existed between fluorescence intensity and elastic modulus when evaluated over the full scan region (PCM + ECM) when compared with PCM points or ECM points alone (figure 6). Overall, the weakest relationships were observed in deep zone scan regions.

PCM elastic moduli exhibited no significant differences among the superficial (68 ± 5 kPa), middle (56 ± 4 kPa) and deep (58 ± 6 kPa) zones ($p = 0.21$, figure 7). In the superficial zone, PCM regions exhibited lower elastic moduli than immediately adjacent regions lacking type VI collagen (figure 8, $p < 0.05$). Elastic moduli reached values comparable to the ECM 2.5 μm from the PCM outer edge. In the middle zone, PCM elastic moduli were lower than those in regions greater than 1 μm from the PCM outer edge ($p < 0.05$). Middle zone elastic moduli reached ECM moduli 1.5 μm from the PCM outer edge. In the deep zone, PCM moduli exhibited lower values than regions greater than 1.5 μm from the PCM outer edge ($p < 0.05$) and ECM-like elastic moduli were observed immediately outside the PCM. In all three zones, ECM elastic moduli were greater than their respective PCM moduli (figure 7, $p < 0.05$). The superficial zone exhibited higher ECM moduli when compared with the middle and deep zones (figure 7, $p < 0.05$).

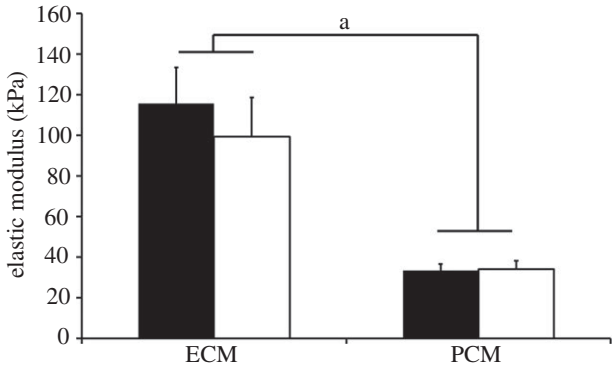

Figure 4. Elastic moduli of ECM and PCM regions measured in the middle/deep zone of unlabelled (black) and IF-labelled (white) cartilage sections. No difference in moduli was observed with IF-labelling in either region ($p = 0.39$ for ECM, $p = 0.97$ for PCM). ECM elastic moduli were significantly greater than PCM moduli in both unlabelled and IF-labelled cartilage sections (a: $p < 0.001$). Moduli presented as mean ± s.e. ($N = 3$, $n = 17$).

4. DISCUSSION

Our results demonstrate that the biomechanical properties of the cartilage PCM correlate with the presence of type VI collagen in the chondrocyte microenvironment. Control experiments verified that immunolabelling had no effect on micromechanical properties of either the cartilage PCM or ECM. Immunolabelling in combination with AFM-based stiffness mapping revealed co-localization of type VI collagen and lower elastic moduli in the PCM. Matrix regions lacking type VI collagen immediately adjacent to the PCM exhibited higher elastic moduli than regions positive for type VI collagen. PCM elastic moduli measured *in situ*

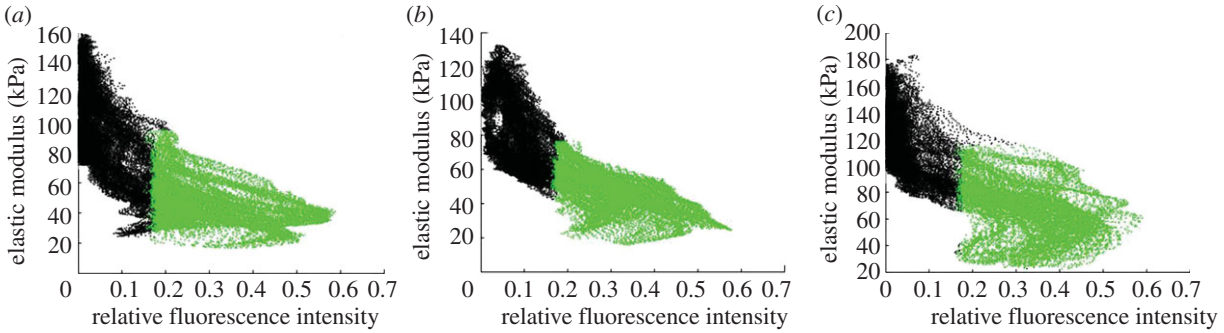

Figure 5. Representative scatter plots of elastic modulus versus relative fluorescence intensity in PCM scan regions in the (*a*) superficial, (*b*) middle and (*c*) deep zones. Regions positive for type VI collagen are designated in green and regions lacking type VI collagen are designated in black. Regions with higher relative fluorescence in IF-positive regions for type VI collagen exhibited lower elastic moduli. (Online version in colour.)

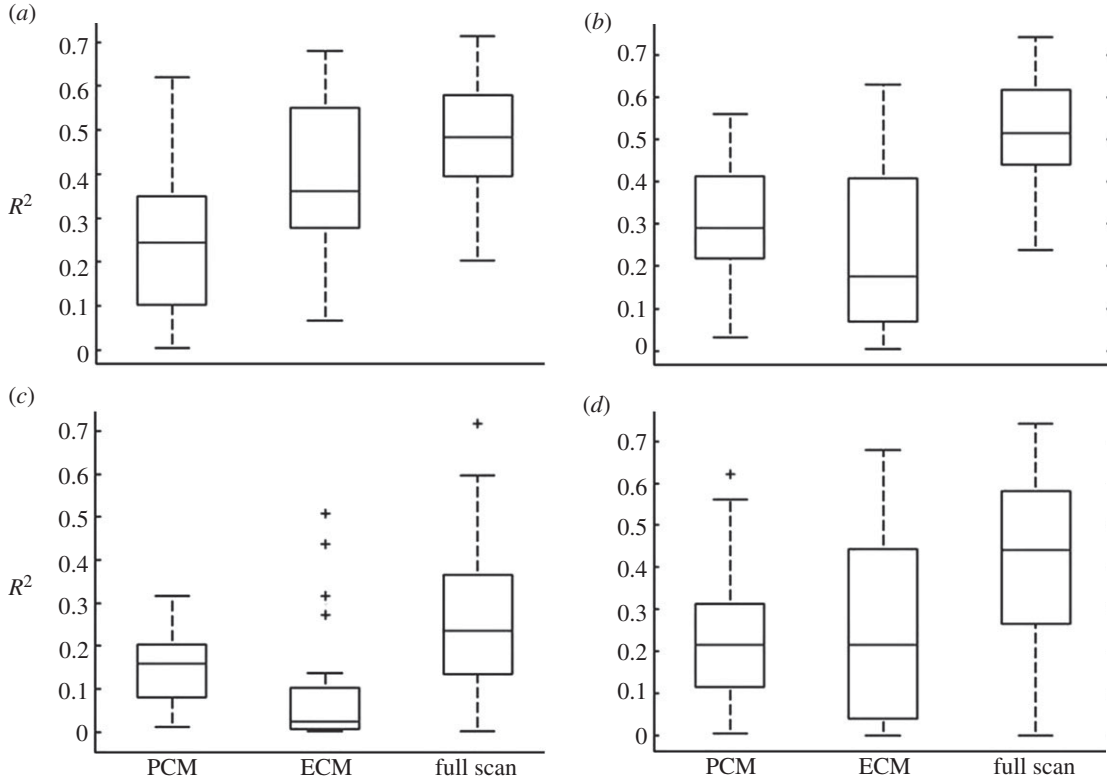

Figure 6. Box plots of coefficient of determination (r^2) for linear regression of elastic modulus versus relative fluorescence intensity for each PCM scan region in the (*a*) superficial, (*b*) middle, (*c*) deep zones and (*d*) across all zones. Separate regression analyses were performed on PCM regions alone, ECM regions alone and the full scan region (PCM + ECM). Median r^2 value is designated by the horizontal line within each box.

exhibited zonal uniformity across the superficial, middle and deep zones of the cartilage.

By evaluating PCM mechanical properties within the context of the local ECM with minimal disruption of native matrix integration, the method presented here provides a direct means to fully evaluate the micromechanical environment of the chondrocyte *in situ*. Stiffness mapping demonstrated that type VI collagen is a defining factor for both the biochemical and biomechanical definitions of the PCM. PCM regions were softer than immediately adjacent regions lacking type VI collagen. In the superficial and middle zones, these regions exhibited intermediate elastic moduli between the PCM and ECM. This result suggests that the territorial matrix, located between the PCM and ECM [12], may serve as a mechanical as well as a structural transition region in articular cartilage. In addition, fluorescence intensity of type VI collagen IF labelling was found to be a significant predictor of elastic modulus. The strongest relationships, based on r^2 values, were observed when evaluated over the full scan region, with fluorescence intensity contributing to 48 per cent, 51 per cent and 23 per cent of the observed variation in elastic modulus in the superficial, middle and deep zones, respectively. Not surprising, the weakest relationships were observed in the deep zone

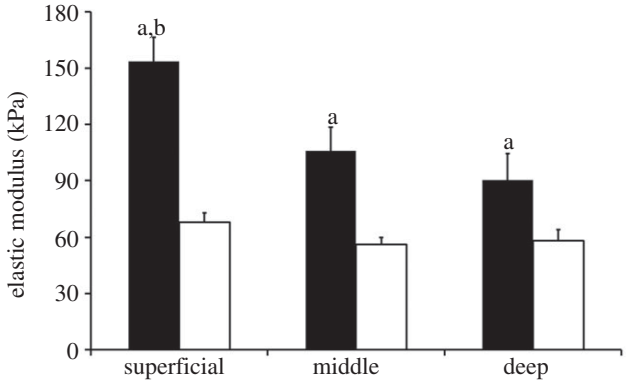

Figure 7. Elastic moduli of ECM (black) and PCM (white) regions measured in the superficial, middle and deep zones of articular cartilage. PCM elastic moduli exhibited zonal uniformity ($p = 0.21$). ECM elastic moduli in all zones were greater than their respective PCM moduli (a: $p < 0.05$). Superficial zone ECM elastic moduli were greater than middle and deep zone ECM moduli (b: $p < 0.05$). Moduli presented as mean ± s.e. ($N = 5$, $n = 20$ per zone).

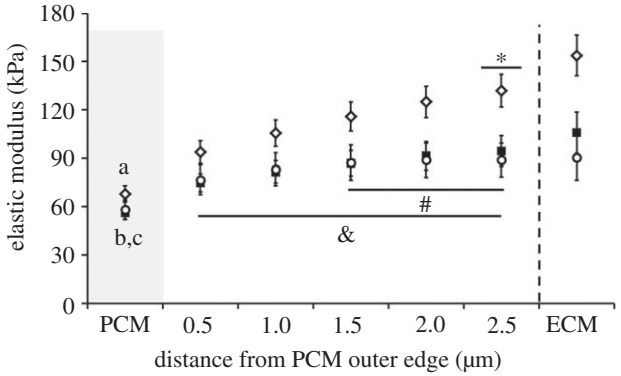

Figure 8. Outward stiffness progression of elastic moduli from the PCM outer edge to the ECM in the superficial (open diamonds), middle (filled squares) and deep (open circles) zones. In the superficial zone, PCM moduli were less than moduli in all regions beyond the PCM outer edge (a: $p < 0.05$) and elastic moduli reached ECM values 2.5 μm from the PCM outer edge ($*p > 0.05$ when compared with ECM). In the middle zone, PCM moduli were less than moduli in regions greater than 1.0 μm from the PCM outer edge (b: $p < 0.05$) and elastic moduli reached ECM values 1.5 μm from the PCM outer edge ($\#p > 0.05$ when compared with ECM). In the deep zone, PCM moduli were less than moduli in regions greater than 1.5 μm from the PCM outer edge (c: $p < 0.05$) and elastic moduli reached ECM values at the PCM outer edge ($\&p > 0.05$ when compared with ECM). Moduli presented as mean ± s.e. ($N = 5$, $n = 20$ per zone).

where the difference between PCM and ECM elastic moduli was the smallest. This observation further supports the defining role of type VI collagen in the biomechanical properties of the PCM.

The results of this study provide evidence for site-specific variations of the elastic modulus within the PCM. For example, the PCM elastic moduli in this study (56–68 kPa) were approximately twice as stiff as those measured *in situ* via AFM for porcine cartilage (approx. 30 kPa) in our previous study [38]. This difference in moduli was not an effect of immunolabelling on microscale stiffness. Rather, it likely reflects a more accurate definition of the PCM boundary that is based on type VI collagen IF, rather than distance from the chondrocyte. When the same 1 μm-thick, distance-based definition of the PCM was employed in the current work, the measured values of PCM elastic moduli (33–34 kPa) were in direct agreement with those in our previous results. The distribution of type VI collagen around cell-sized voids demonstrated that this distance-based definition underestimated the true local PCM thickness. It is also possible that type VI collagen extends beyond the PCM and into the adjacent territorial matrix, where it was reported to be interwoven with type II collagen fibrils [55]. Inclusion of higher modulus territorial matrix regions may have contributed to elevated PCM moduli. Furthermore, there are limitations in lateral resolution associated with the use of micrometer-sized indenters for AFM-based stiffness mapping of soft substrates [56]. For spherical probes, the contact radius scales with tip radius and indentation depth. Because stiffness maps were collected using a single force trigger (300 nN), indentation depths were smaller in stiffer ECM regions (approx. 800 nm) than in softer PCM regions (approx. 1.5 μm). As a result, contact radii were larger in PCM regions (2.0–2.2 μm) when compared with ECM regions (1.5–1.8 μm). Indenter contact with adjacent territorial matrix and/or ECM regions might contribute to artificial stiffening of peripheral PCM regions.

PCM elastic moduli measured in this current study are in excellent agreement with those measured using other techniques such as micropipette aspiration of isolated chondrons [34–36]. In particular, a recent study reported the mechanical properties of the PCM in intact cartilage by employing inverse boundary element analysis coupled with three-dimensional confocal microscopy of compressed porcine cartilage. This study estimated the Young modulus of the PCM to be 24–59 kPa in the middle zone [37]. The consistency in PCM properties among these different measurement techniques suggests that the sample preparation methods in this study (i.e. frozen sectioning and immunolabelling) do not have significant effects on PCM properties.

Previous studies investigating zonal variations in PCM properties focused on mechanically extracting chondrons from the superficial and middle/deep zones of the tissue [34–36]. Results from these micropipette aspiration studies and our *in situ* work agree that the PCM exhibits zonal uniformity in its mechanical properties. Zonal uniformity in PCM properties coupled with zonal differences in chondrocyte [32,33] and ECM [29,30] properties generates depth-dependent variations in the ratio of chondrocyte to PCM to ECM properties, which in turn influence the local mechanical and physiochemical environments of the cell [16,17]. This result supports the hypothesized role of the PCM as a mechanical transducer that provides a uniform cellular environment throughout the tissue depth, despite large inhomogeneities in local strain during joint loading [23].

While type VI collagen is often used as the primary marker of the cartilage PCM, a recent study by Alexopoulos *et al.* [57] demonstrated that intact chondrons could be isolated from Col6a1 knockout mice that lack type VI collagen. A number of matrix molecules are also found either exclusively or at higher concentrations in the PCM when compared with the surrounding ECM, including perlecan [58,59], hyaluronan [60,61], biglycan [62], type IX collagen [63], fibronectin [64] and laminin [65]. The fact that intact chondrons can be isolated from Col6a1 null mice [57] suggests that other molecular components likely contribute to the structural integrity and biomechanical properties of the PCM, potentially providing alternative composition-based definitions of the PCM.

Consistent with other AFM studies [46,66], ECM modulus values observed in our study were lower than macroscale values for healthy porcine articular cartilage [67,68]. Measured ECM moduli were greater than those previously reported for the superficial zone (154 kPa versus 44 kPa) of porcine patellar cartilage [66] and the middle/deep zone (90–106 kPa versus 81 kPa) of porcine articular cartilage [38]. Furthermore, the observed ECM microscale elastic properties decreased with depth from the articular surface. This observation is inconsistent with the depth-dependent increase in ECM compressive properties observed in macroscale studies [29,30]. These observations may be attributed to the fact that the AFM measures highly localized properties that may be dominated by individual molecular components of the tissue. Previous work by Loparic *et al.* [49], on the nanostiffness of porcine articular cartilage, demonstrated that proteoglycans *in situ* are an order of magnitude softer than collagen fibres. In the cartilage ECM, proteoglycan content increases with depth from the articular surface [25]. Interstitial fluid pressurization in response to AFM microindentation is minimal [46], with an estimated relaxation time constant of approximately 60 ms on the basis of moduli presented in our study. Consistent with previous AFM nano- and microindentation studies [69], ECM elastic moduli increased slightly with increasing indentation velocity from 1 to 25 $\mu m\, s^{-1}$ (see the electronic supplementary material, figure S1). The fact that the effect of indentation rate was relatively small over a large range of rates indicates that the relaxation time of tissue is significantly shorter than the characteristic loading time of these experiments. This suggests that the properties measured using this AFM-based technique represent the intrinsic mechanical properties of the solid matrix independent of biphasic effects. As a result, the apparent softening of the ECM with depth observed in the present work may be due in part to the high concentration of proteoglycans in the middle and deep zones.

Another important difference in these measurements when compared with most previous studies of depth-dependent cartilage properties is that in the current study, cartilage sections were tested in the transverse direction relative to the articular surface. While the mesh-like ultrastructure of the PCM [7,12,27] suggests that the PCM is isotropic, distinct structural anisotropy is present in the ECM owing to the arcade-like architecture of type II collagen fibres [26]. In the superficial zone, collagen fibres are highly aligned parallel to the articular surface. The middle zone is more structurally isotropic with collagen fibres randomly oriented at angles oblique to the articular surface. In the deep zone, collagen fibres are oriented perpendicular to the articular surface. It is possible that the direction of loading relative to the collagen fibre orientation in each zone attributed to the depth-dependent decrease observed in ECM elastic moduli. In addition, macroscale properties of cartilage ECM have been shown to depend on the direction of loading relative to the split-line orientation in the superficial zone [70]. Split-line direction was not taken into account in this study, and the effect of loading relative to the split-line direction on the micromechanical properties of cartilage ECM and PCM has yet to be determined.

In summary, our findings provide further support for type VI collagen as a defining factor both in the biochemical and biomechanical definitions of the PCM and the biomechanical role of the PCM in articular cartilage. In addition, our findings provide a more complete characterization of matrix mechanical properties in the cellular microenvironment and suggest that the territorial matrix serves as a mechanical as well as a structural transition between the cartilage PCM and ECM. The combined approach of immunolabelling and AFM stiffness mapping used in this study provides a novel means for characterization of the relationship between tissue biochemical composition and biomechanical properties *in situ*.

This work was supported in part by a National Science Foundation Graduate Research Fellowship (R.E.W.) and National Institutes of Health grants nos AG15768, AR50245, AR48182, AR48852 and AR055659.

REFERENCES

1 Mow, V. C., Bachrach, N. M., Setton, L. A. & Guilak, F. 1994 Stress, strain, pressure, and flow fields in articular cartilage and chondrocytes. In *Cell mechanics and cellular engineering* (eds V. C. Mow, F. Guilak, R. Tran-Son-Tay & R. M. Hochmuth), pp. 345–379. New York, NY: Springer.

2 Lai, W. M., Sun, D. D., Ateshian, G. A., Guo, X. E. & Mow, V. C. 2002 Electrical signals for chondrocytes in cartilage. *Biorheology* **39**, 39–45.

3 Mow, V. C. & Guo, X. E. 2002 Mechano-electrochemical properties of articular cartilage: their inhomogeneities and anisotropies. *Annu. Rev. Biomed. Eng.* **4**, 175–209. (doi:10.1146/annurev.bioeng.4.110701.120309)

4 Guilak, F., Sah, R. L. & Setton, L. A. 1997 Physical regulation of cartilage metabolism. In *Basic orthopaedic biomechanics*, 2nd edn. (eds V. C. Mow & W. C. Hayes), pp. 179–207. Philadelphia, PA: Lippincott-Raven Publishers.

5 Williams, G. M., Chan, E. F., Temple-Wong, M. M., Bae, W. C., Masuda, K., Bugbee, W. D. & Sah, R. L. 2010 Shape, loading, and motion in the bioengineering design, fabrication, and testing of personalized synovial joints. *J. Biomech.* **43**, 156–165. (doi:10.1016/j.jbiomech.2009.09.021)

6 Grodzinsky, A. J., Levenston, M. E., Jin, M. & Frank, E. H. 2000 Cartilage tissue remodeling in response to

mechanical forces. *Annu. Rev. Biomed. Eng.* **2**, 691–713. (doi:10.1146/annurev.bioeng.2.1.691)
7 Poole, C. A., Flint, M. H. & Beaumont, B. W. 1987 Chondrons in cartilage: ultrastructural analysis of the pericellular microenvironment in adult human articular cartilages. *J. Orthop. Res.* **5**, 509–522. (doi:10.1002/jor.1100050406)
8 Poole, C. A., Ayad, S. & Schofield, J. R. 1988 Chondrons from articular cartilage: I. Immunolocalization of type VI collagen in the pericellular capsule of isolated canine tibial chondrons. *J. Cell Sci.* **90**, 635–643.
9 Poole, C. A., Ayad, S. & Gilbert, R. T. 1992 Chondrons from articular cartilage. V. Immunohistochemical evaluation of type VI collagen organisation in isolated chondrons by light, confocal and electron microscopy. *J. Cell Sci.* **103**, 1101–1110.
10 Hagiwara, H., Schroter-Kermani, C. & Merker, H. J. 1993 Localization of collagen type VI in articular cartilage of young and adult mice. *Cell Tissue Res.* **272**, 155–160. (doi:10.1007/BF00323581)
11 Youn, I., Choi, J. B., Cao, L., Setton, L. A. & Guilak, F. 2006 Zonal variations in the three-dimensional morphology of the chondron measured *in situ* using confocal microscopy. *Osteoarthritis Cartilage* **4**, 889–897. (doi:10.1016/j.joca.2006.02.017)
12 Poole, C. A., Flint, M. H. & Beaumont, B. W. 1984 Morphological and functional interrelationships of articular cartilage matrices. *J. Anat.* **138**, 113–138.
13 Poole, C. A. 1997 Articular cartilage chondrons: form, function and failure. *J. Anat.* **191**, 1–13. (doi:10.1046/j.1469-7580.1997.19110001.x)
14 Hunziker, E. B., Quinn, T. M. & Hauselmann, H. J. 2002 Quantitative structural organization of normal adult human articular cartilage. *Osteoarthritis Cartilage* **10**, 564–572. (doi:10.1053/joca.2002.0814)
15 Guilak, F., Alexopoulos, L. G., Upton, M. L., Youn, I., Choi, J. B., Cao, L., Setton, L. A. & Haider, M. A. 2006 The pericellular matrix as a transducer of biomechanical and biochemical signals in articular cartilage. *Ann. N.Y. Acad. Sci.* **1068**, 498–512. (doi:10.1196/annals.1346.011)
16 Guilak, F. & Mow, V. C. 2000 The mechanical environment of the chondrocyte: a biphasic finite element model of cell–matrix interactions in articular cartilage. *J. Biomech.* **33**, 1663–1673. (doi:10.1016/S0021-9290(00)00105-6)
17 Alexopoulos, L. G., Setton, L. A. & Guilak, F. 2005 The biomechanical role of the chondrocyte pericellular matrix in articular cartilage. *Acta Biomater.* **1**, 317–325. (doi:10.1016/j.actbio.2005.02.001)
18 Michalek, A. J. & Iatridis, J. C. 2007 A numerical study to determine pericellular matrix modulus and evaluate its effects on the micromechanical environment of chondrocytes. *J. Biomech.* **40**, 1405–1409. (doi:10.1016/j.jbiomech.2006.05.025)
19 Korhonen, R. K. & Herzog, W. 2008 Depth-dependent analysis of the role of collagen fibrils, fixed charges and fluid in the pericellular matrix of articular cartilage on chondrocyte mechanics. *J. Biomech.* **41**, 480–485. (doi:10.1016/j.jbiomech.2007.09.002)
20 Knight, M. M., Lee, D. A. & Bader, D. L. 1998 The influence of elaborated pericellular matrix on the deformation of isolated articular chondrocytes cultured in agarose. *Biochim. Biophys. Acta* **1405**, 67–77. (doi:10.1016/S0167-4889(98)00102-5)
21 Knight, M. M., Ross, J. M., Sherwin, A. F., Lee, D. A., Bader, D. L. & Poole, C. A. 2001 Chondrocyte deformation within mechanically and enzymatically extracted chondrons compressed in agarose. *Biochim. Biophys. Acta* **1526**, 141–146. (doi:10.1016/S0304-4165(01)00118-0)
22 Hing, W. A., Sherwin, A. F. & Poole, C. A. 2002 The influence of the pericellular microenvironment on the chondrocyte response to osmotic challenge. *Osteoarthritis Cartilage* **10**, 297–307. (doi:10.1053/joca.2002.0517)
23 Choi, J. B., Youn, I., Cao, L., Leddy, H. A., Gilchrist, C. L., Setton, L. A. & Guilak, F. 2007 Zonal changes in the three-dimensional morphology of the chondron under compression: the relationship among cellular, pericellular, and extracellular deformation in articular cartilage. *J. Biomech.* **40**, 2596–2603. (doi:10.1016/j.jbiomech.2007.01.009)
24 Nicodemus, G. D. & Bryant, S. J. 2008 The role of hydrogel structure and dynamic loading on chondrocyte gene expression and matrix formation. *J. Biomech.* **41**, 1528–1536. (doi:10.1016/j.jbiomech.2008.02.034)
25 Venn, M. & Maroudas, A. 1977 Chemical composition and swelling of normal and osteoarthrotic femoral head cartilage. I. Chemical composition. *Ann. Rheum. Dis.* **36**, 121–129. (doi:10.1136/ard.36.2.121)
26 Hwang, W. S., Li, B., Jin, L. H., Ngo, K., Schachar, N. S. & Hughes, G. N. 1992 Collagen fibril structure of normal, aging, and osteoarthritic cartilage. *J. Pathol.* **167**, 425–433. (doi:10.1002/path.1711670413)
27 Hunziker, E. B., Michel, M. & Studer, D. 1997 Ultrastructure of adult human articular cartilage matrix after cryotechnical processing. *Microsc. Res. Tech.* **37**, 271–284. (doi:10.1002/(SICI)1097-0029(19970515)37:4<271::AID-JEMT3>3.0.CO;2-O)
28 Quinn, T. M., Hunziker, E. B. & Hauselmann, H. J. 2005 Variation of cell and matrix morphologies in articular cartilage among locations in the adult human knee. *Osteoarthritis Cartilage* **13**, 672–678. (doi:10.1016/j.joca.2005.04.011)
29 Schinagl, R. M., Gurskis, D., Chen, A. C. & Sah, R. L. 1997 Depth-dependent confined compression modulus of full-thickness bovine articular cartilage. *J. Orthop. Res.* **15**, 499–506. (doi:10.1002/jor.1100150404)
30 Chen, S. S., Falcovitz, Y. H., Schneiderman, R., Maroudas, A. & Sah, R. L. 2001 Depth-dependent compressive properties of normal aged human femoral head articular cartilage: relationship to fixed charge density. *Osteoarthritis Cartilage* **9**, 561–569. (doi:10.1053/joca.2001.0424)
31 Tomkoria, S., Patel, R. V. & Mao, J. J. 2004 Heterogeneous nanomechanical properties of superficial and zonal regions of articular cartilage of the rabbit proximal radius condyle by atomic force microscopy. *Med. Eng. Phys.* **26**, 815–822. (doi:10.1016/j.medengphy.2004.07.006)
32 Darling, E. M., Zauscher, S. & Guilak, F. 2006 Viscoelastic properties of zonal articular chondrocytes measured by atomic force microscopy. *Osteoarthritis Cartilage* **14**, 571–579. (doi:10.1016/j.joca.2005.12.003)
33 Shieh, A. C. & Athanasiou, K. A. 2006 Biomechanics of single zonal chondrocytes. *J. Biomech.* **39**, 1595–1602. (doi:10.1016/j.jbiomech.2005.05.002)
34 Guilak, F., Alexopoulos, L. G., Haider, M. A., Ting-Beall, H. P. & Setton, L. A. 2005 Zonal uniformity in mechanical properties of the chondrocyte pericellular matrix: micropipette aspiration of canine chondrons isolated by cartilage homogenization. *Ann. Biomed. Eng.* **33**, 1312–1318. (doi:10.1007/s10439-005-4479-7)
35 Alexopoulos, L. G., Haider, M. A., Vail, T. P. & Guilak, F. 2003 Alterations in the mechanical properties of the human chondrocyte pericellular matrix with osteoarthritis. *J. Biomech. Eng.* **125**, 323–333. (doi:10.1115/1.1579047)

36 Alexopoulos, L. G., Williams, G. M., Upton, M. L., Setton, L. A. & Guilak, F. 2005 Osteoarthritic changes in the biphasic mechanical properties of the chondrocyte pericellular matrix in articular cartilage. *J. Biomech.* **38**, 509–517. (doi:10.1016/j.jbiomech.2004.04.012)

37 Kim, E., Guilak, F. & Haider, M. A. 2010 An axisymmetric boundary element model for determination of articular cartilage pericellular matrix properties *in situ* via inverse analysis of chondron deformation. *J. Biomech. Eng.* **132**, 031011. (doi:10.1115/1.4000938)

38 Darling, E. M., Wilusz, R. E., Bolognesi, M. P., Zauscher, S. & Guilak, F. 2010 Spatial mapping of the biomechanical properties of the pericellular matrix of articular cartilage measured *in situ* via atomic force microscopy. *Biophys. J.* **98**, 2848–2856. (doi:10.1016/j.bpj.2010.03.037)

39 Radmacher, M., Tillamnn, R. W., Fritz, M. & Gaub, H. E. 1992 From molecules to cells: imaging soft samples with the atomic force microscope. *Science* **257**, 1900–1905. (doi:10.1126/science.1411505)

40 Gad, M., Itoh, A. & Ikai, A. 1997 Mapping cell wall polysaccharides of living microbial cells using atomic force microscopy. *Cell Biol. Int.* **21**, 697–706. (doi:10.1006/cbir.1997.0214)

41 A-Hassan, E., Heinz, W. F., Antonik, M. D., D'Costa, N. P., Nageswaran, S., Schoenenberger, C. A. & Hoh, J. H. 1998 Relative microelastic mapping of living cells by atomic force microscopy. *Biophys. J.* **74**, 1564–1578. (doi:10.1016/S0006-3495(98)77868-3)

42 Lewis, N. T., Hussain, M. A. & Mao, J. J. 2008 Investigation of nano-mechanical properties of annulus fibrosus using atomic force microscopy. *Micron* **39**, 1008–1019. (doi:10.1016/j.micron.2007.08.009)

43 Hu, K., Radhakrishnan, P., Patel, R. V. & Mao, J. J. 2001 Regional structural and viscoelastic properties of fibrocartilage upon dynamic nanoindentation of the articular condyle. *J. Struct. Biol.* **136**, 46–52. (doi:10.1006/jsbi.2001.4417)

44 Allen, D. M. & Mao, J. J. 2004 Heterogeneous nanostructural and nanoelastic properties of pericellular and interterritorial matrices of chondrocytes by atomic force microscopy. *J. Struct. Biol.* **145**, 196–204. (doi:10.1016/j.jsb.2003.10.003)

45 Radhakrishnan, P., Lewis, N. T. & Mao, J. J. 2004 Zone-specific micromechanical properties of the extracellular matrices of growth plate cartilage. *Ann. Biomed. Eng.* **32**, 284–291. (doi:10.1023/B:ABME.0000012748.41851.b4)

46 Park, S., Costa, K. D., Ateshian, G. A. & Hong, K. S. 2009 Mechanical properties of bovine articular cartilage under microscale indentation loading from atomic force microscopy. *Proc. Inst. Mech. Eng. H* **223**, 339–347.

47 Stolz, M. *et al.* 2009 Early detection of aging cartilage and osteoarthritis in mice and patient samples using atomic force microscopy. *Nat. Nanotechnol.* **4**, 186–192. (doi:10.1038/nnano.2008.410)

48 Desrochers, J., Amrein, M. A. & Matyas, J. R. 2010 Structural and functional changes of the articular surface in a post-traumatic model of early osteoarthritis measured by atomic force microscopy. *J. Biomech.* **43**, 3091–3098. (doi:10.1016/j.jbiomech.2010.08.009)

49 Loparic, M., Wirz, D., Daniels, A. U., Raiteri, R., Vanlandingham, M. R., Guex, G., Martin, I., Aebi, U. & Stolz, M. 2010 Micro- and nanomechanical analysis of articular cartilage by indentation-type atomic force microscopy: validation with a gel–microfiber composite. *Biophys. J.* **98**, 2731–2740. (doi:10.1016/j.bpj.2010.02.013)

50 Moreno Flores, S. & Toca-Herrera, J. L. 2009 The new future of scanning probe microscopy: combining atomic force microscopy with other surface-sensitive techniques, optical microscopy and fluorescence techniques. *Nanoscale* **1**, 40–49. (doi:10.1039/b9nr00156e)

51 Sen, S. & Kumar, S. 2009 Combining mechanical and optical approaches to dissect cellular mechanobiology. *J. Biomech.* **43**, 45–54. (doi:10.1016/j.jbiomech.2009.09.008)

52 Mow, V. C., Kuei, S. C., Lai, W. M. & Armstrong, C. G. 1980 Biphasic creep and stress relaxation of articular cartilage in compression: theory and experiments. *J. Biomech. Eng.* **102**, 73–84. (doi:10.1115/1.3138202)

53 Guo, S. & Akhremitchev, B. B. 2006 Packing density and structural heterogeneity of insulin amyloid fibrils measured by AFM nanoindentation. *Biomacromolecules* **7**, 1630–1636. (doi:10.1021/bm0600724)

54 Abebe, E. S., Moorman III, C. T., Dziedzic, T. S., Spritzer, C. E., Cothran, R. L., Taylor, D. C., Garrett Jr, W. E. & DeFrate, L. E. 2009 Femoral tunnel placement during anterior cruciate ligament reconstruction: an *in vivo* imaging analysis comparing transtibial and 2-incision tibial tunnel-independent techniques. *Am. J. Sports Med.* **37**, 1904–1911. (doi:10.1177/0363546509340768)

55 Soder, S., Hambach, L., Lissner, R., Kirchner, T. & Aigner, T. 2002 Ultrastructural localization of type VI collagen in normal adult and osteoarthritic human articular cartilage. *Osteoarthritis Cartilage* **10**, 464–470. (doi:10.1053/joca.2002.0512)

56 Radmacher, M., Fritz, M. & Hansma, P. K. 1995 Imaging soft samples with the atomic force microscope: gelatin in water and propanol. *Biophys. J.* **69**, 264–270. (doi:10.1016/S0006-3495(95)79897-6)

57 Alexopoulos, L. G., Youn, I., Bonaldo, P. & Guilak, F. 2009 Developmental and osteoarthritic changes in Col6a1-knockout mice: biomechanics of type VI collagen in the cartilage pericellular matrix. *Arthritis Rheum.* **60**, 771–779. (doi:10.1002/art.24293)

58 SundarRaj, N., Fite, D., Ledbetter, S., Chakravarti, S. & Hassell, J. R. 1995 Perlecan is a component of cartilage matrix and promotes chondrocyte attachment. *J. Cell Sci.* **108**, 2663–2672.

59 Melrose, J., Roughley, P., Knox, S., Smith, S., Lord, M. & Whitelock, J. 2006 The structure, location, and function of perlecan, a prominent pericellular proteoglycan of fetal, postnatal, and mature hyaline cartilages. *J. Biol. Chem.* **281**, 36 905–36 914. (doi:10.1074/jbc.M608462200)

60 Knudson, C. B. 1993 Hyaluronan receptor-directed assembly of chondrocyte pericellular matrix. *J. Cell Biol.* **120**, 825–834. (doi:10.1083/jcb.120.3.825)

61 Cohen, M., Klein, E., Geiger, B. & Addadi, L. 2003 Organization and adhesive properties of the hyaluronan pericellular coat of chondrocytes and epithelial cells. *Biophys. J.* **85**, 1996–2005. (doi:10.1016/S0006-3495(03)74627-X)

62 Kavanagh, E. & Ashhurst, D. E. 1999 Development and aging of the articular cartilage of the rabbit knee joint: distribution of biglycan, decorin, and matrilin-1. *J. Histochem. Cytochem.* **47**, 1603–1616. (doi:10.1177/002215549904701212)

63 Poole, C. A., Gilbert, R. T., Herbage, D. & Hartmann, D. J. 1997 Immunolocalization of type IX collagen in normal and spontaneously osteoarthritic canine tibial cartilage and isolated chondrons. *Osteoarthritis Cartilage* **5**, 191–204. (doi:10.1016/S1063-4584(97)80014-3)

64 Chang, J., Nakajima, H. & Poole, C. A. 1997 Structural colocalisation of type VI collagen and fibronectin in agarose cultured chondrocytes and isolated chondrons extracted from adult canine tibial cartilage. *J. Anat.* **190**, 523–532. (doi:10.1046/j.1469-7580.1997.19040523.x)

65 Durr, J., Lammi, P., Goodman, S. L., Aigner, T. & von der Mark, K. 1996 Identification and immunolocalization of

laminin in cartilage. *Exp. Cell Res.* **222**, 225–233. (doi:10.1006/excr.1996.0028)

66 Coles, J. M., Blum, J. J., Jay, G. D., Darling, E. M., Guilak, F. & Zauscher, S. 2008 *In situ* friction measurement on murine cartilage by atomic force microscopy. *J. Biomech.* **41**, 541–548. (doi:10.1016/j.jbiomech.2007.10.013)

67 Fermor, B., Christensen, S. E., Youn, I., Cernanec, J. M., Davies, C. M. & Weinberg, J. B. 2007 Oxygen, nitric oxide and articular cartilage. *Eur Cell Mater.* **13**, 56–65.

68 Hennerbichler, A., Rosenberger, R., Arora, R. & Hennerbichler, D. 2008 Biochemical, biomechanical and histological properties of osteoarthritic porcine knee cartilage: implications for osteochondral transplantation. *Arch. Orthop. Trauma Surg.* **128**, 61–70. (doi:10.1007/s00402-007-0360-5)

69 Han, L., Frank, E. H., Greene, J. J., Lee, H. Y., Hung, H. H., Grodzinsky, A. J. & Ortiz, C. 2011 Time-dependent nanomechanics of cartilage. *Biophys. J.* **100**, 1846–1854. (doi:10.1016/j.bpj.2011.02.031)

70 Chahine, N. O., Wang, C. C., Hung, C. T. & Ateshian, G. A. 2004 Anisotropic strain-dependent material properties of bovine articular cartilage in the transitional range from tension to compression. *J. Biomech.* **37**, 1251–1261. (doi:10.1016/j.jbiomech.2003.12.008)